Chapter 10
Acoustic Emission Dynamics Initiated by Fluid Infusion on Laboratory Scale

A. Ponomarev, G. Sobolev, and Yu. Maibuk

10.1 Introduction

The influence of water on the increase of seismic activity has been investigated in various seismotectonic environments, including the observations of the processes of reservoir filling [Gupta, 1992; Simpson et al., 1988; Mirzoyev et al., 1988; Sobolev, 1993]. The physical interpretation considered was mainly related to increase of pore pressure and the corresponding decrease of effective pressure according to modified Coulomb-Moore law [Brace, Martin, 1968]. This effect is the basis of the Dilatation-Diffusion (DD) model of the earthquake preparation [Scholz et al., 1973]. Quantitative estimates of the dependence of this effect on various values of lithostatic and hydrostatic pressure, temperature and rock permeability were made in [Miller et al., 1999]. A review of possible induced seismicity mechanisms can be found in the special issue of *Pure Appl. Geophys.* [Trifu (ed.), 2002]. The fractal properties of the water-induced seismicity are investigated in [Smirnov, 1994]. Connection of local seismic activity and small changes of water level in the reservoir (phase synchronization) were detected in [Peinke et al, 2006]. It should be noted that small changes in pore pressure also correlate with the variations of small earthquakes activity. It is shown that seismicity in the zone adjacent to lake Baikal depends on the seasonal variations of the water level in the lake, which change the pore pressure by several millibars [Djadkov, 1997]. This paper investigates the influence of relatively low water inflow on the acoustic emission in compressed samples.

A. Ponomarev (✉), G. Sobolev, and Y. Maibuk
Schmidt Institute of Physics of the Earth, Russian Academy of Sciences, Moscow, Russia
e-mail: avp@ifz.ru

V. de Rubeis et al. (eds.), *Synchronization and Triggering: from Fracture to Earthquake Processes*, GeoPlanet: Earth and Planetary Sciences 1,
DOI 10.1007/978-3-642-12300-9_10,

10.2 Experiment procedure

The biaxial compression experiments were conducted on samples consisting of basalt sand and cement. The detailed description can be found in [Sobolev, Ponomarev, 1997; Sobolev, Ponomarev, 2003]. The model has the form of an edge brick: base of 205 mm, thickness of 85 mm, side of 266 mm, the angle between the long side and base 25°. The model consisted of 3 equal-size layers parallel to the slanted sides. Two outer layers had higher durability than the central one: therefore, the inner layer was more prone to destruction. Basalt gravel with sizes from 2 to 20 mm was added to the inner layer. Initial values of P-wave velocities were 3.5 km/sec in the outer layers and 1.7 km/sec in the inner layer.

Experiments were conducted on a mechanical (lever) press which can maintain constant load over extended periods of time. The lateral load normal to the slanted sides, was kept constant for all experiments at the level of 4 tons. The vertical load F was increased stepwise by adding loads on the long arm of the lever. We call these actions the "mechanical load-ons". After each load step, the model was kept stable for 1-3 days, while the acoustic emission caused by the load-on decreased to the background levels.

Acoustic emission (AE) was collected by the 10-channel acquisition system A–Line32D (manufactured by "INTERUNIS", Russia). The dynamic range was 96 dB, sampling frequency was 5 MHz, and acoustic passband was 30-500 KHz. Besides AE, the vertical load and mechanical shortening of the model were measured and recorded every 10 seconds. The results presented here were obtained in the course of experiments with 2 identical models. During the final stage of the loading of the first model, when the vertical load exceeded 95%, water was infused into the model. The 5 mm diameter hole was drilled to a depth of 10 cm, the hole opening being located on the upper side. The hole was cased with a polyethylene tube except for the lowest 5 mm, so the water penetrated the model only in hole-bottom area. The 5 ml volumes of water which equaled to ∼0.1% of the model volume were kept constant during the experiments. Figure 10.1a shows the view of the model in the press, Fig. 10.1b shows the plot of vertical load F during two consecutive infusions of water. Infusion of water caused significant increases of AE activity, thus we will call these actions "initiations" infusion.

10.3 Experiment results

10.3.1 Initiation #1

Figure 10.2 shows the AE dynamics in the lower (I) and in the upper (II) parts of the model. The initiation hole was located in the upper part. The starting point of the X-axis corresponds to the moment of mechanical load-on. At this moment, the load increased by 1.6% (up to 97% of the rupturing load). The water was infused into the

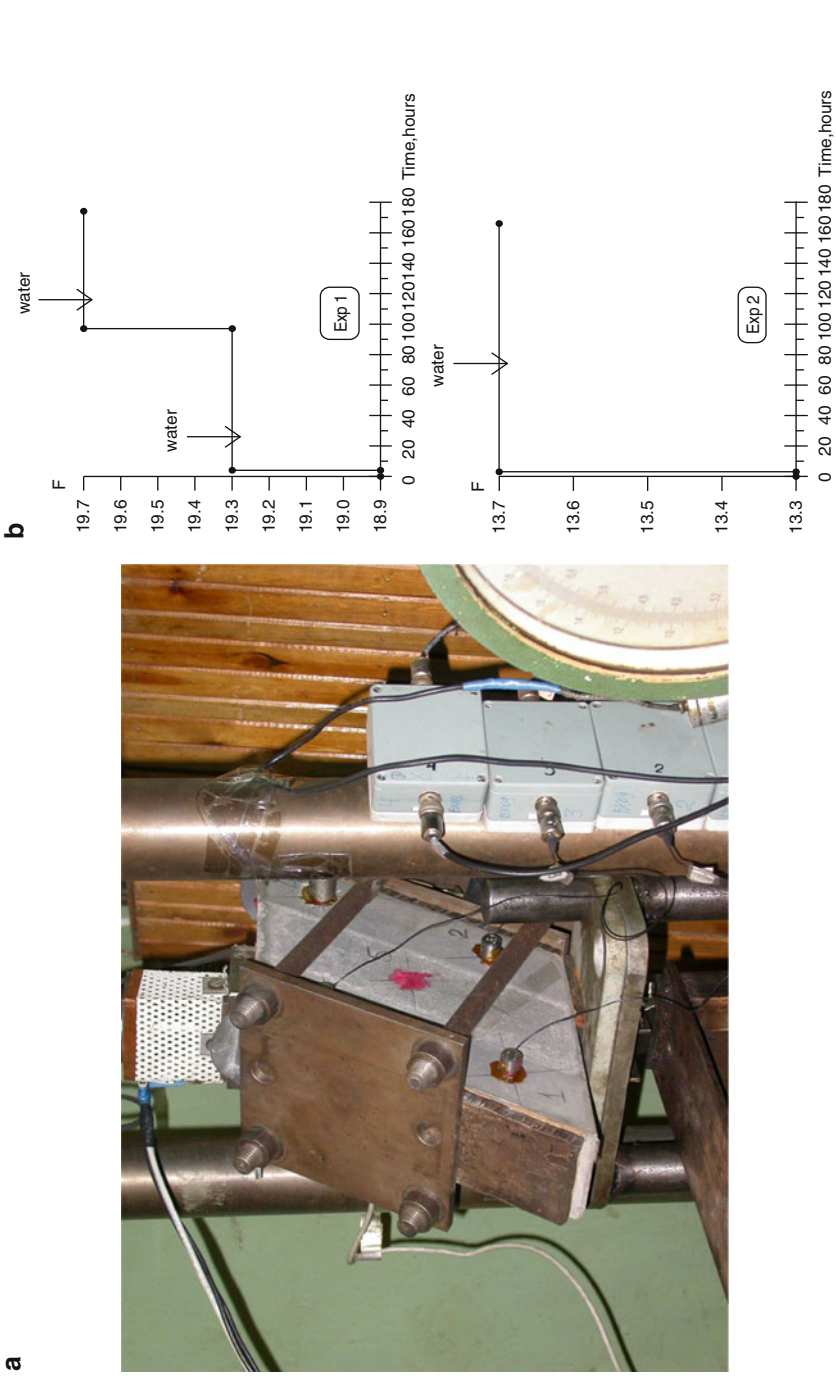

Fig. 10.1 General layout of the experiment with the model in the press (**a**) and the diagram of load F at the moments of water infusion (**b**). The arrows indicate the moments of water infusion during experiments with the 1st model (#1, #2) and with the 2nd model (#3)

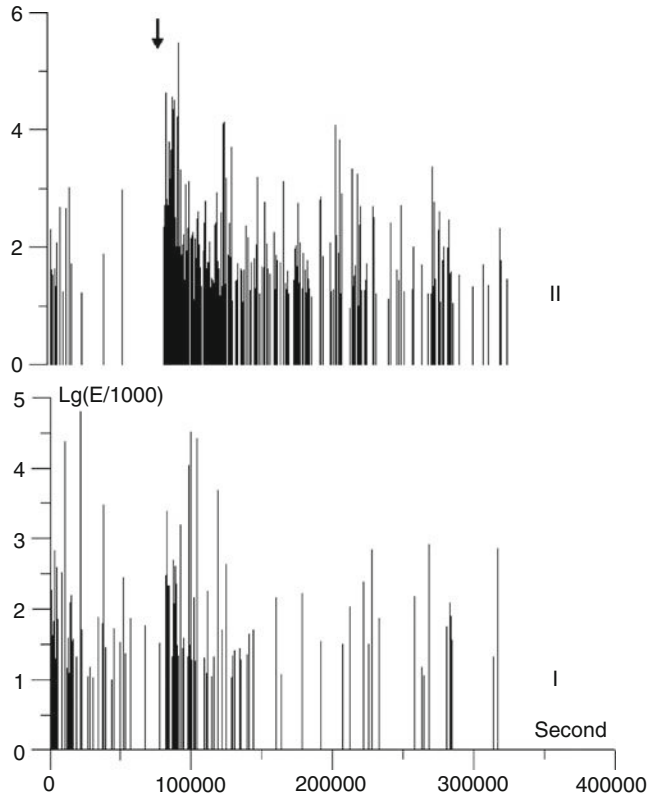

Fig. 10.2 The sequence of AE signals and their energy E in the zones I and II during the experiment with Initiation #1. The arrow indicates the start of water infusion

hole at 80828th second (marked by an arrow) and was absorbed by the model during 24 minutes (1440 seconds). Energy of AE events was estimated as the square of amplitude of signal from the sensor nearest to the hypocenter. Averaging of energy by all sensors reduced the computational stability due to the following two reasons. First, the number of sensors used for hypocenter location varied from 4 to 8. Second, with increasing distance between the sensor and the hypocenter, the frequency and amplitude of the signal changed significantly due to absorption and scattering of acoustic waves. A comparison of the upper and lower plots in Fig. 10.2 definitely shows a considerable increase of AE activity following the water infusion into the upper part of the model.

The epicenters of acoustic signals on the two faces of the model are shown in Fig. 10.3. The two lower diagrams correspond to the time span between the load-on F and the water infusion; the duration is 80827 seconds. The two upper diagrams correspond to the time span after water infusion (80828 sec. – 323768 sec. in Fig. 10.2, this is 67.48 hours). The following details must be noted: the intensity of signals increased significantly in the upper part (II), and also, whereas the

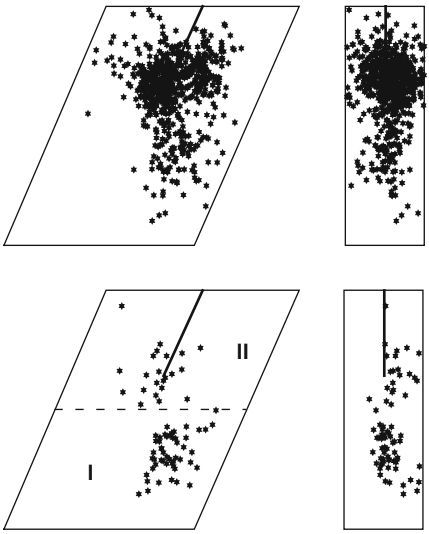

Fig. 10.3 Locations of the AE epicenters onto the front side and the perpendicular side during the experiment with Initiation #1; lower plot – before the infusion, upper plot – after the infusion. The dotted line separates the model into zones I and II. Solid straight lines show the hole projection onto the faces of the model

strongest acoustic events before water infusion happened in the lower part of the model, the strongest activity migrated to the upper part of the model following the water infusion (Fig. 10.2). The sources of acoustic signals were located inside the model, i.e., the internal cracking took place. Usually during the loading of specimens many cracks occur on the edges. In the current experiments, the internal cracking, which better corresponds to the processes of earthquake origination, was achieved due to lower durability of the inner layer of the model.

Now let us consider in greater detail the time interval immediately following the water infusion. First signals in zone II were detected just 19 seconds after infusion while in zone I scarce acoustic signals emitted only after 1308 s. In our previous paper [Sobolev, Ponomarev et al., 2006] it was discovered that penetration of water into the tip of an active crack causes an acoustic signal (crack extension) with the time delay of no more than 5 seconds. The data on the first interval in Fig. 10.2 shows that before the water infusion area I exhibited even greater acoustic activity than area II, i.e., there appeared to be more active cracks. Thus, the 1308 second delay can be interpreted as the time needed for water to come to the remote area. The low acoustic activity can be explained by the fact that, given the small amount of water injected (0.1% of the model volume), the water did not penetrate all active cracks in the area. At the same time the emergence of acoustic signals after 1308 seconds in the area I can be attributed to the influence of water. The indirect evidence of this can be found in the results of AE locations. The hypocenters of the signals on the upper plots in Fig. 10.3 are located in the upper part of this area (I), i.e., closer to the hole than it is the case before the water infusion (lower plots in Fig. 10.3).

The hypocenters of the first signals emerging in zone II immediately after the water infusion in the time span of the first hundreds of seconds are located at

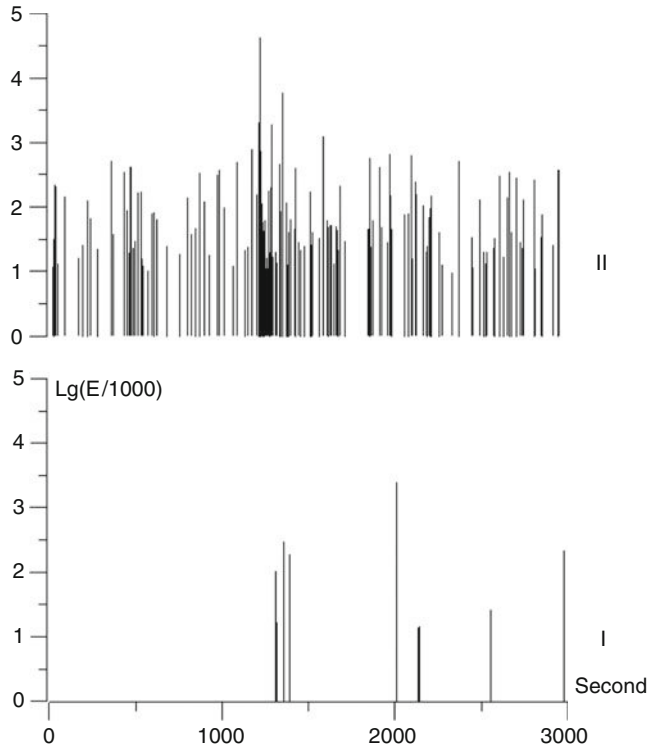

Fig. 10.4 Sequence of AE signals and their energies in the zones I and II after water infusion in the experiment with Initiation #1

30-50 mm distances from the hole. In Fig. 10.3 one can see a cluster group of high energy signals in the interval 1212–1225 seconds from the moment of water infusion. Their sources lie at 40-60 mm distances from the hole; the strongest signal (E = 4.63) occurred close to the middle of the group; its coordinates are x = 153 mm, y = 40 mm, z = 160 mm.

10.3.2 Initiation #2

The second infusion of water into the hole was conducted 4 days after the first one. The starting point of X-axis in Fig. 10.5 corresponds to the moment of load-on while F was increased by 2%. The total resulting load was equal to 20.1 tons, which is 0.5 tons above the level maintained during the Initiation #1. The moment of water infusion is marked by the arrow. Time interval between the moment of load-on and the moment of water infusion was 62760 seconds (17.43 hours). The water was

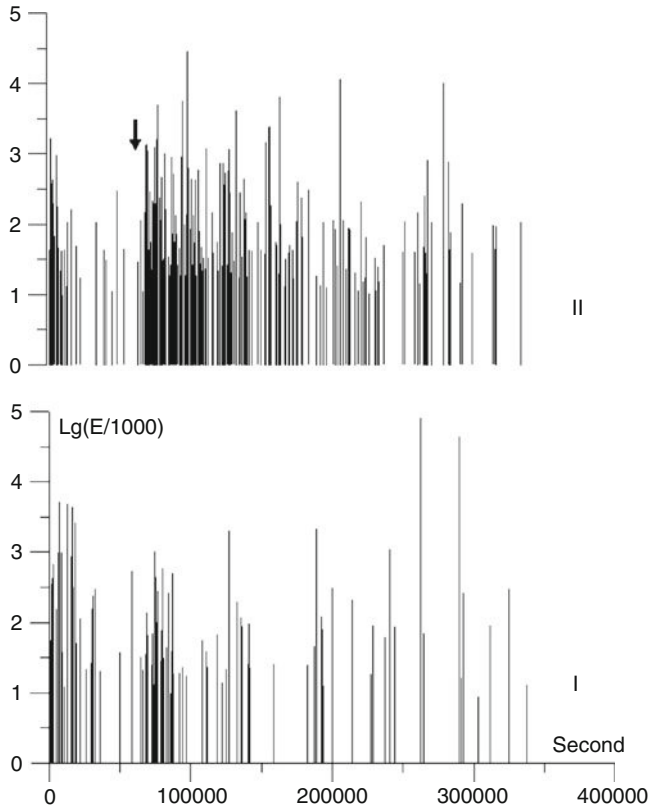

Fig. 10.5 The sequence of AE signals and their energy E in the zones I and II during the experiment with Initiation #2. The arrow indicates the start of water infusion

absorbed by the sample through the hole-bottom area after 38 minutes, which is 16 minutes longer than for the previous initiation. There can be two possible reasons for this effect. First, the moisture content of the model in the area adjacent to the hole-bottom was elevated compared to the initial one as a result of the previous initiation. Second, the number of active cracks where the water is actively absorbed could decrease as a result of the first initiation. Figure 10.5 shows that in the second initiation, just like it happened in the first one, the inflow of water resulted in the increase of AE activity.

The lower plots in Fig. 10.6 show the epicenters of the AE events occurring between the mechanical load-on and water infusion; the upper plots show the AE activity during 274610 seconds following the water infusion. Most events occurred in the area adjacent to the hole-bottom.

As one of significant differences between Initiations #1 and #2, we can mention the lower number of AE signals occurring in the upper area (II) after water infusion. So, during the same $\Delta T = 48$ hour interval, 548 AE signals occurred in Initiation

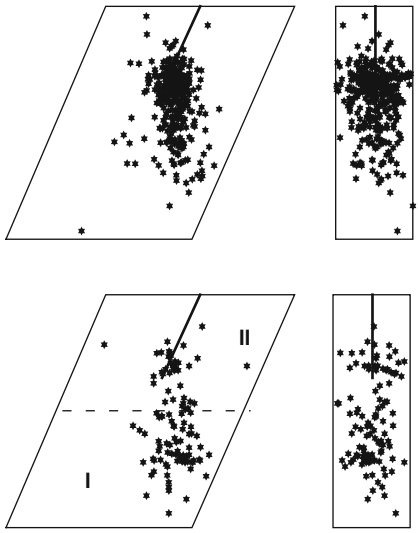

Fig. 10.6 Locations of the AE epicenters onto the front side (slanted) and the perpendicular side during the experiment with Initiation # 2; lower plot – before the infusion, upper plot – after the infusion. The dotted line separates the model into areas I and II. Solid straight lines show the hole projection onto the faces of the model

#1, whereas only 255 occurred in Initiation #2. At the same time, the AE activity in the remote area (I) was comparable in both Initiations.

The second notable difference is that in Initiation #2 the delays between the water infusion and the start of AE pulses were longer and practically identical in both parts of the model. This is shown in Fig. 10.7 where the events are plotted on a more detailed time scale following the moment of water infusion. One can see significant differences compared with Fig. 10.4. In the first case, the delays were 19 and 1308 seconds, in the second case being 2219 and 2000 seconds.

10.3.3 Initiation #3

It was interesting to find out whether the AE initiation effect would occur with the lower stresses applied to the model, and whether there is any difference in the manifestation of the effect. This was performed in experiment #2. The water was infused when the load F equaled 13.8 tons, i.e., the load was 70% of the critical instead of 97% in the previous experiment. The water infusion started 256683 seconds (71.3 hours) after the mechanical load-on by 3.4%. The water was absorbed slower than in Initiation #1 (2 hours versus 24 minutes). This difference is probably explained by the fact that the lower stress resulted in lower number of water-containing microcracks. Figure 10.8 shows the significant increase in AE activity around the hole location II; this area also exhibits the strongest events.

Figure 10.9 shows the epicenters of the AE events before water infusion (lower plots) and after infusion (upper plots). One can see the increased density of events

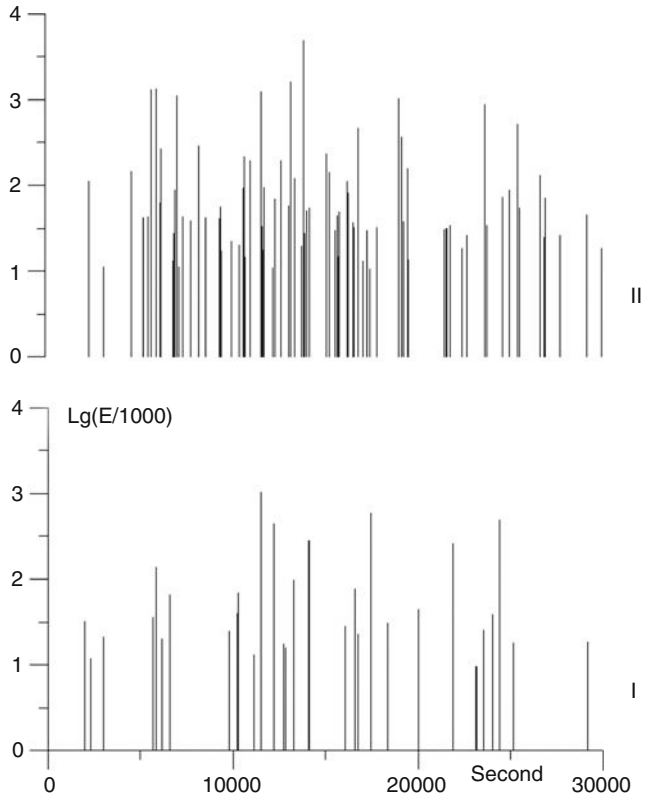

Fig. 10.7 Sequence of AE signals and their energies in the zones I and II after water infusion in the experiment with Initiation #2

around the hole location in area II after water infusion. Before the water infusion, the events occurred practically with the same density in the upper and lower parts of the model. The sources of AE signals were located inside the model, i.e., it was internal cracking again.

Figure 10.10 shows an expanded plot of the interval immediately following the water infusion; significant time delays of AE events relative to the moment of water infusion are observed in both areas. First AE signals in area II emerge after 1909 seconds (32 min.), in area I the delay is 4269 seconds (71 min.). Since the intensity of AE activity had been comparable in both areas prior to water infusion, it is reasonable to assume that the greater delay in area I is basically the delay of water arrival in the remote area. The lower AE activity compared to Initiation #1 is probably caused by smaller number of active microcracks accumulated inside the model by the moment of Initiation #3. Hypocenter locations of the first AE events emerging in area I after water infusion show that these hypocenters are located close to the upper limit of this area at 40-50 mm distances from the hole-bottom.

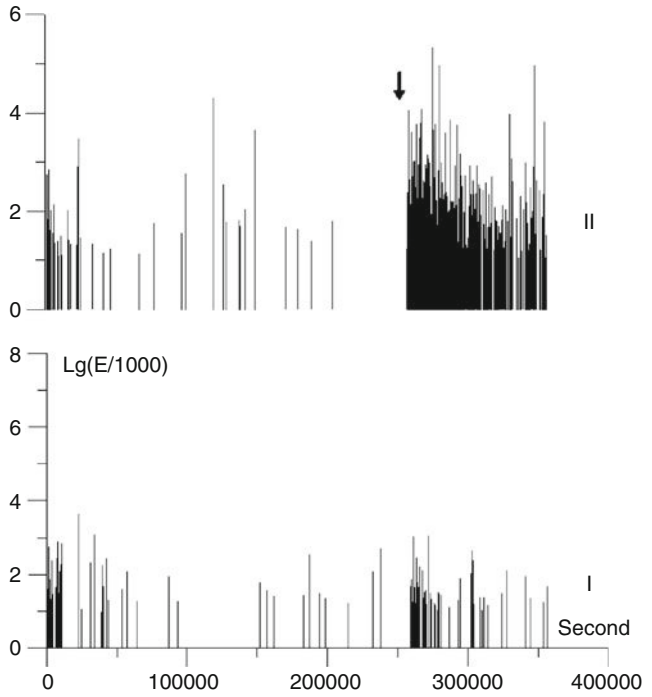

Fig. 10.8 The sequence of AE signals and their energy E in the areas I and II during the experiment with Initiation # 3. The arrow indicates the start of water infusion

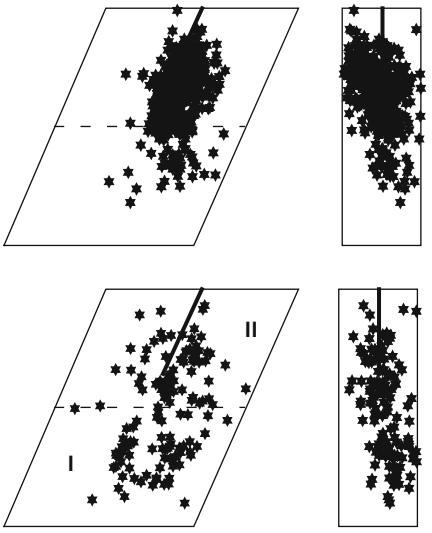

Fig. 10.9 Locations of the AE signal epicenters onto the front side (slanted) and the perpendicular side during the experiment with Initiation # 3; lower plot – before the infusion, upper plot – after the infusion. The dotted line separates the model into zones I and II. Solid straight lines show the hole projection onto the faces of the model

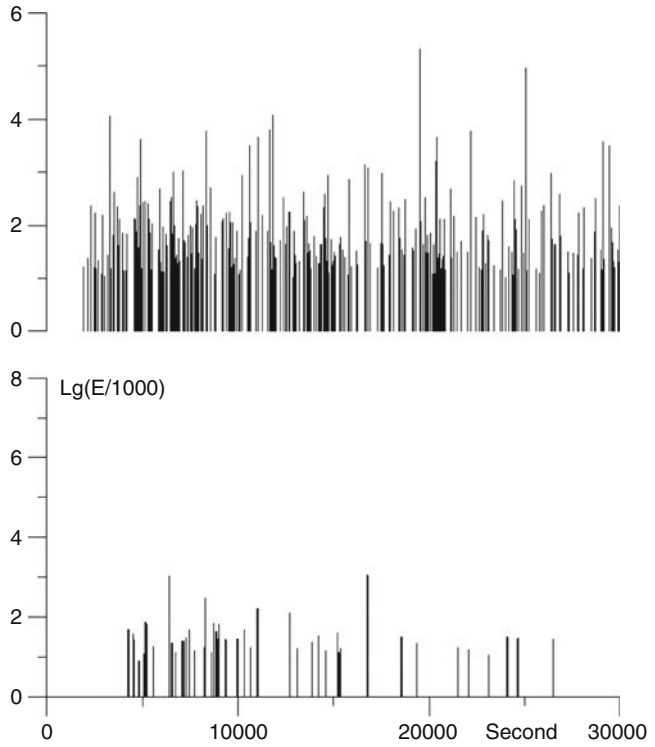

Fig. 10.10 Sequence of AE signals and their energies in the zones I and II after water infusion in the experiment with Initiation #3

10.4 Discussion

From Figs. 10.2, 10.5, and 10.8 it follows that the patterns of AE relaxation after mechanical load-ons and after water infusions are substantially different. In the first case, the high activity decreased significantly during several hundreds of seconds following the load-on. In the second case, the elevated activity was maintained at a high level during several thousands of seconds. Additionally, this elevated activity did emerge with a certain time delay relative to water infusion; see Figs. 10.4, 10.7, and 10.10.

Another aspect of this difference in AE patterns can be seen in Figs. 10.11 and 10.12. In these figures the rate of change of AE activity dN/dt is plotted for the cases of mechanical load (lower plots) and for water infusions during Initiations #1 and #3 (upper plots). The number of events was divided by the time interval dt, which was incremented logarithmically.

In both cases of AE excitation by a mechanical load-on, the relaxation process conforms to the Omori law (slanted lines in the lower plots).

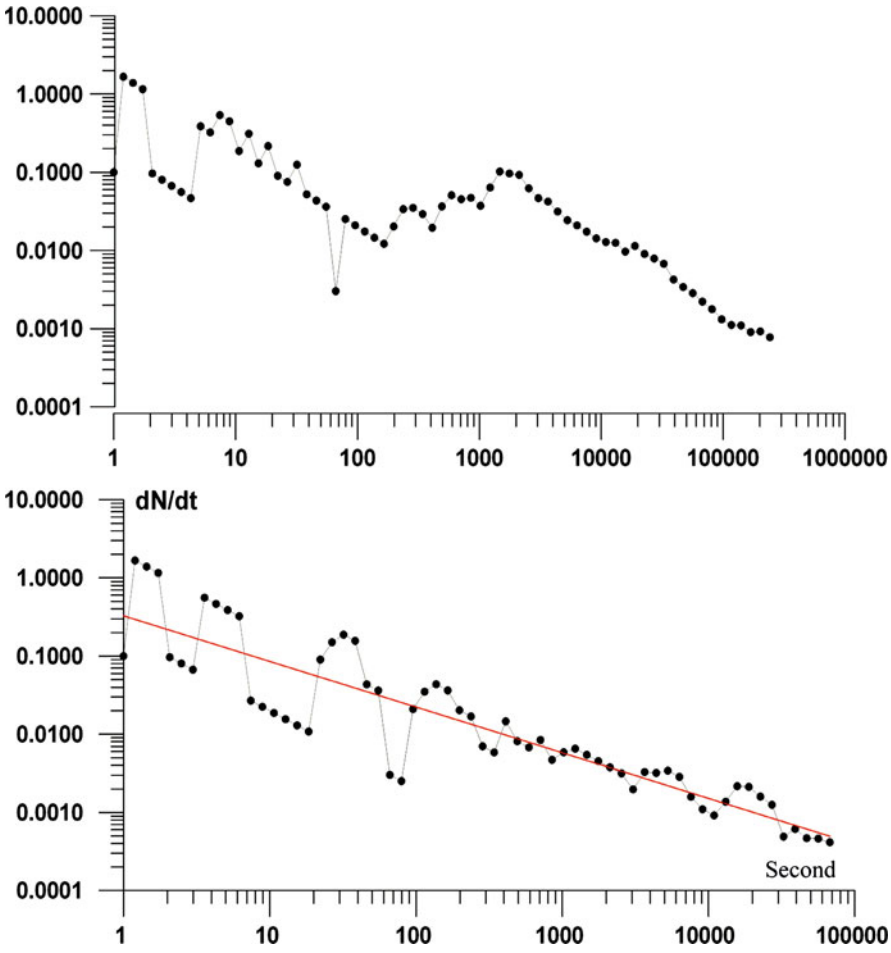

Fig. 10.11 Changes in the rate of AE activity dN/dt (per second) during the experiment with Initiation #1. The lower plot shows the reaction to mechanical load-on, the upper plot – the reaction to water infusion

$$dN/dt = C/(1+t)^{p} \tag{10.1}$$

In particular, the "log-log" plot (a) in Fig. 10.11 corresponds to the equation

$$dN/dt = 0.32/(1+t)^{0.58} \tag{10.2}$$

with the determination factor $R = 0.81$, whereas plot (a) in Fig 10.12 corresponds to the equation

$$dN/dt = 1.1/(1+t)^{0.66}; \quad R = 0.88 \tag{10.3}$$

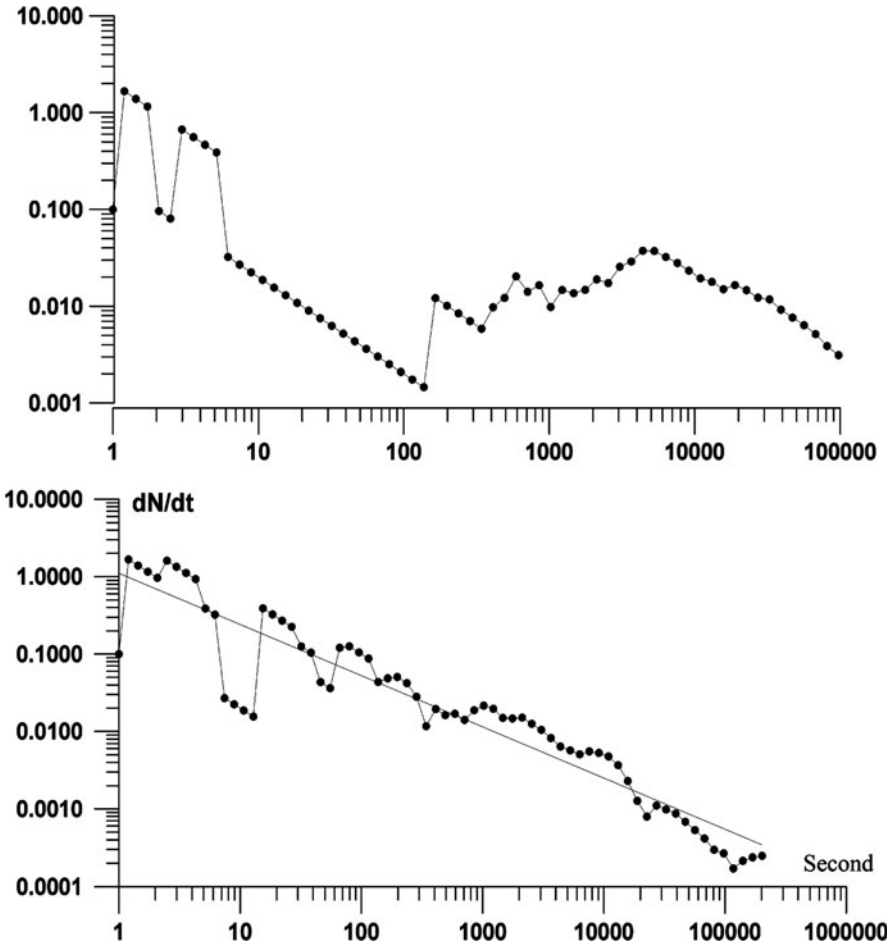

Fig. 10.12 Changes in the rate of AE activity dN/dt (per second) during the experiment with Initiation #3. The lower plot shows the reaction to mechanical load-on, the upper plot – the reaction to water infusion

As it was already noted, the AE activity after water infusion occurred with a certain time delay. Let us consider the process after the activity emergence — plots (b) in Figs. 10.11 and 10.12. In both cases, during Initiations #1 and #3 the AE activity decreased during the first 100 seconds after the emergence of the initial signals; this was followed by a gradual activity increase and subsequent decrease. This pattern cannot be described in terms of relaxation equation type (10.1). During Initiation #2 the dynamic pattern was basically similar; however, it was not processed statistically due to lower number of AE signals.

The decay in the activity within a short time interval, covering the first 100 s, is hardly connected with the process of water infusion, which lasted dozens of minutes. The physical sense of the decay in the acoustic activity is not clear so far.

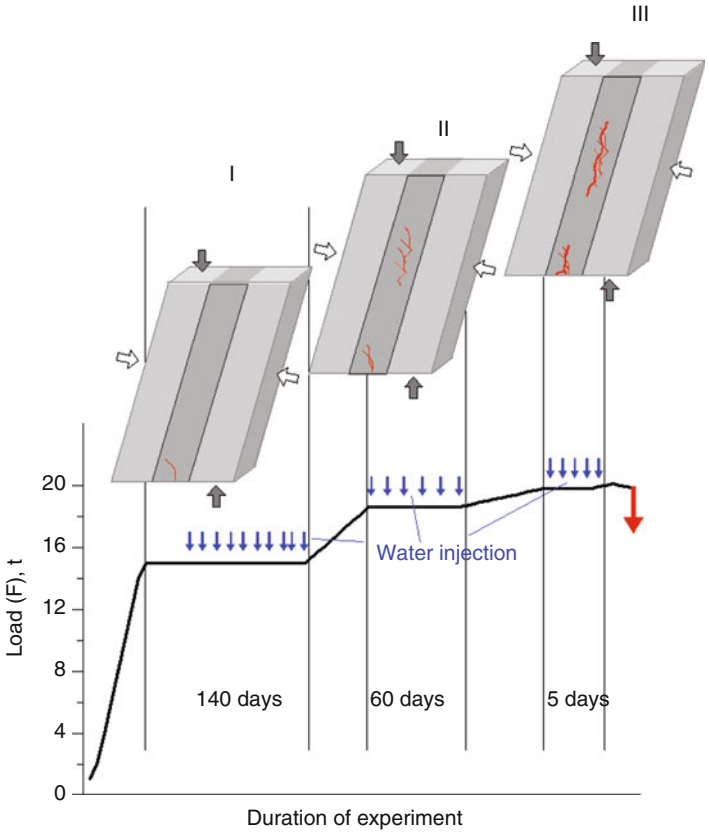

Fig. 10.13 Layout of the experiment for water infusion into the cracks at different stages of loading, I, II, and III, with the increasing load F on the model

In our previous paper [Sobolev, Ponomarev et al., 2006] the influence of water injected directly into the cracks visible on the surface on the AE activity was investigated; the model was similar in composition to the one described here. In Fig. 10.13 one can see the layout of that experiment which lasted for more than 7 months. As an example, Fig. 10.14 shows the dynamics of the AE response to the water infusion during stages I, II, III corresponding to increasing values of load F. It was determined that the patterns of gradual increase and subsequent decrease of AE activity can be described by the formula

$$dN/dt = (dN/dt)_0 \cdot \exp[\phi(t) - \Psi(t)] \tag{10.4}$$

where the terms in the exponent expression are time dependent. Variations in experimental data are accounted for by adjustment of factors a, k and V in the formula

$$dN/dt = a \cdot \exp[t^k - V/(1+t)^m] \tag{10.5}$$

The physical interpretation of these effects must take into account several concurrent processes. The increased rate of cracking can be caused by the decrease of durability of the moistened area, by an increase of brittleness, or by an increase of stresses. The effect of durability decrease in solids caused by absorption, chemisorptions, wetting and other physical-chemical processes was discovered for solids of various compositions (Rehbinder effect). This effect was discovered also for rocks [Rehbinder, Schukin, 1972; Traskin et al, 1989]. The effect is caused by a decrease of the free surface energy U on the liquid-solid surface. As determined by the spectral analysis, the chemical composition of the model includes: MgO, Al_2O_3, SiO_2, P_2O_5, K_2O, CaO, TiO_2, Cr_2O_3, MnO, FeO. The chemical composition of the water used in the experiments includes: HCO_3, Cl, SO_4, NO_3, NO_2, Na, Ca, Mg, NH_4.

Intensified destruction of brittle solids under the influence of surfactants absorbed on the surfaces of the cracks is quantitatively treated in [Kornev, 2003]. However, the manifestation of this effect must gradually decrease due to the limited number of cracks in metastable state, due to decrease of accumulated potential energy as a result of AE, and due to exhaustion of water which causes the AE activation.

We support the hypothesis that the number of cracks in metastable state is a significant, and possibly the crucial factor determining the AE dynamics after an external influence. The number of such cracks grows together with the growth of the applied loads and (or) with the increased duration of load application. This can be seen, for example, in the changes of curves plotted in Fig. 10.14. Along with the increase of the load F from stage I to stage III (Fig. 10.13), the AE reaction to the water infusion manifests itself as a general increase in activity and the occurrence of a maximum soon after the infusion. This effect was discovered in various experiments and is described in [Sobolev, Ponomarev et al., 2006]. With the low F values, the AE decrease starts even with the increasing load. With the high F values, the AE maximum occurs after the moment of reaching the maximum value of F and even after the moment when F starts decreasing. The plots in Fig. 10.14 can be adequately described by formula (10.5) under the assumption that the number of active cracks at the current moment t_i is decreased by the number of cracks which had already generated the acoustic signals and had thus become inactive (not stressed to subcritical level), i.e., calculations by formula (10.5) are amended by

$$dN/dt = dN/dt_{(i)} - dN/dt_{(i-1)} \tag{10.6}$$

The structure of formulae (10.4, 10.5) resembles the equation of the kinetic concept of the strength of solids [Zhurkov, 1984]. In the work [Stavrogin and Protosenya, 1985], on the basis of numerous experiments it was established that the creep of different rocks is described by the following equation

$$d\varepsilon/dt = \varepsilon_0 \cdot \exp[(\gamma\sigma - U_0)/KT] \tag{10.7}$$

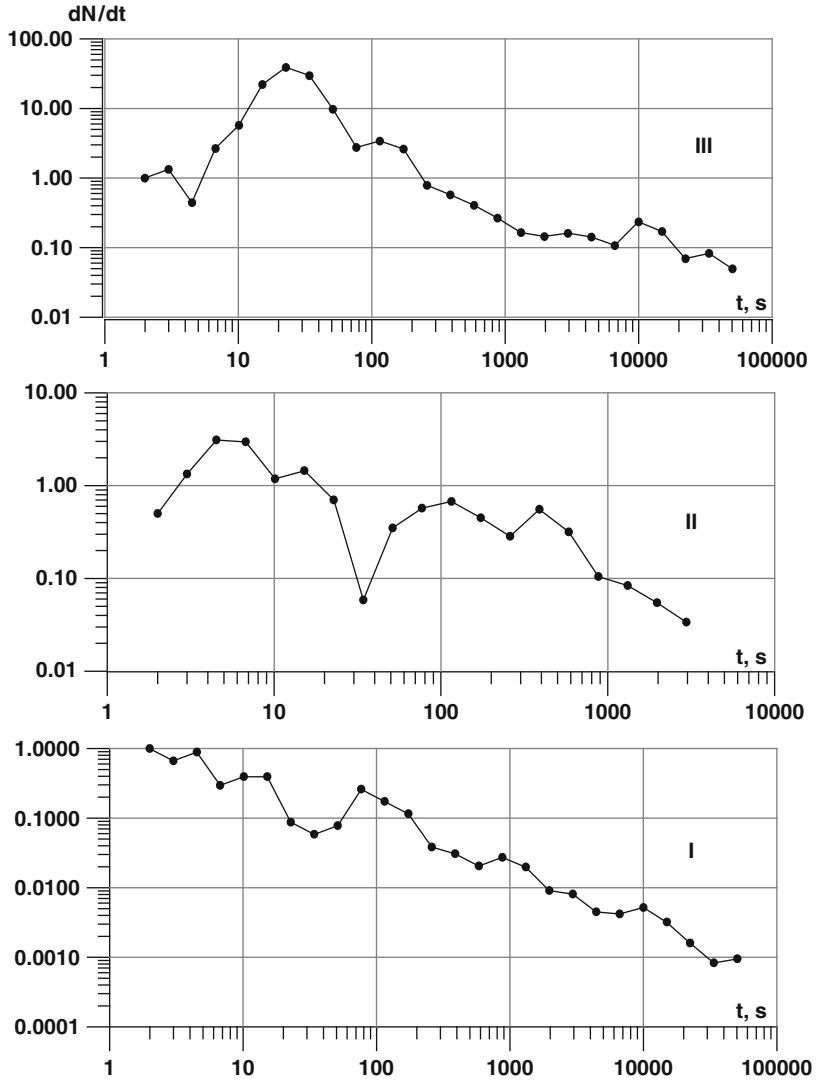

Fig. 10.14 Examples of differential changes of the number of AE events per unit time after water infusion during stages I, II, and III

where ε is the relative deformation, γ the parameter sensitive to structure, σ the applied stress, U_0 the activation energy, K the Boltzmann constant, and T is the absolute temperature.

The parameter ε_0 indicates the maximum possible rate of deformation, which coincides with the velocity of elastic waves. The authors of the work [Tamuzh and Kuksenko, 1978] showed that with a similar type of equation it is possible to describe the rate of destruction. In this case, the parameters of the equation contain

factors describing the gradual weakening in the undistorted bonds, and thus indicative of the increase in the effective stress.

Besides the formal similarity of formulas (10.4), (10.5), and (10.7), there must exist much more profound physical connections. The rate of crack formation in the brittle material (like our models) is roughly proportional to the rate of relative deformation: $dN/dt \sim d\varepsilon/dt$. In case of the initiation of AE by water infusion one can assume that $\gamma\sigma$ increases with time, for example due to the decreased friction along the crack faces and associated growth of stresses in the tips of these cracks. The U_0 value, giving the level of energy barriers, also does not stay constant due to changes in the material strength.

In Fig. 10.15 one can see examples of the use of equations (10.5), and (10.6) for modeling plots of the Fig. 10.14 type. The plotted curve 1 was calculated with the following parameters in (10.5): $a = 10$, $k = 0.005$, $V = 20$, $m = 1$. The low value of k should be noted – it means that the first term in the exponent in (10.4), (10.5), and (10.7) changes insignificantly with time. When $m = 1$, the second term in exponent changes according to the same law as in the Omori equation (10.1). Consequently,

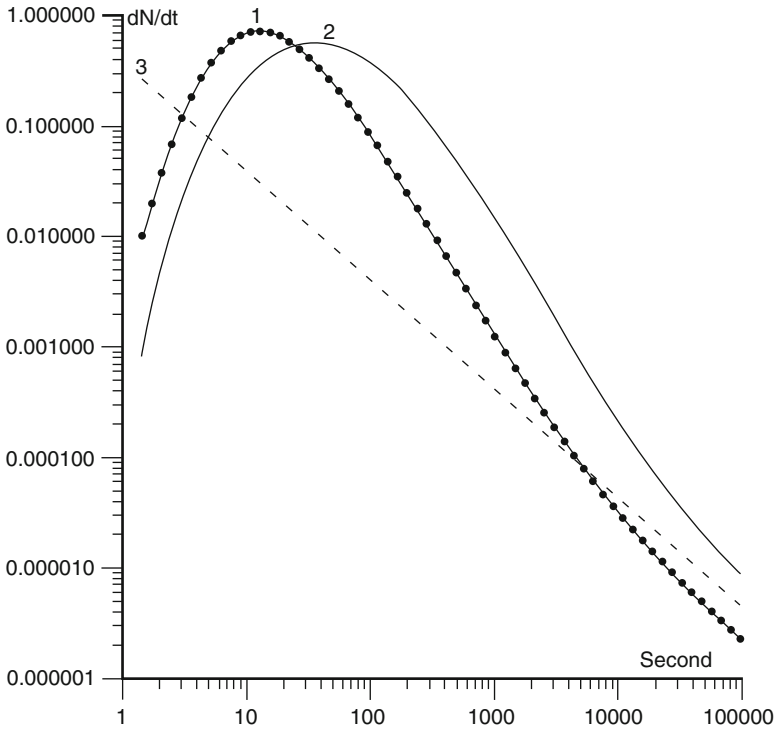

Fig. 10.15 Evaluation of AE dynamics according to formulas (10.5) and (10.6):
1 – parameters: $a = 10$, $k = 0.005$, $V = 20$, $m = 1$;
2 – same values of parameters, but the delay of water arrival to metastable cracks is accounted for;
3 – same values of parameters k and V, but $m = 10^{-6}$, $a = 10^{10}$

the growth or decrease of k results in the growth or decrease of the number of AE signals per unit time, but the time position of the maximum for plot 1 in Fig. 10.15 does not change. On the other hand, the growth or decrease of m results in the shift of the maximum along the time scale. Plot 3 corresponds to the value of $m = 10^{-6}$ with the values of k and V unchanged; the vertical scale is increased by a factor of 10^9. This plot can be described by the equation of type (10.1):

$$dN/dt = 0.38/(1 + t)^{0.98}; \quad R = 0.99 \tag{10.8}$$

Comparing the plots (b) in Figs 10.11, 10.12, and 10.14 it follows that in the current experiment the AE reaction to the water infusion through the hole (Figs. 10.11, 10.12) is reached later than in the previous experiments when water was injected directly into the crack (Fig. 10.14). The probable reason is that water coming through the hole-bottom only gradually reaches the metastable cracks. Plot 2 in Fig. 10.15 shows the shifting and flattening of the maximum in case when calculations are done with the same values of a, k, V, m as for plot 1, but the certain velocity of water propagation after infusion is taken into account. If the calculations by formulas (10.5) – (10.6) are made under the assumption that the water will access the active cracks not immediately, but 10 seconds later, the maximum dN/dt time is shifted from 12.8 sec (plot 1) to 38.3 sec (plot 2). Slower water propagation explains big time delays in plots (b) in Figs 10.11 and 10.12. It should also be noted that after the local maxima, plots (b) in Figs. 10.11 and 10.12 can be quite adequately described by the relaxation equations of type (10.1). The values of parameters p are equal to 1.1 and 0.77, i.e., higher than the corresponding values in equations (10.2) and (10.3). This must be understood as a steeper decrease of AE rate after water initiation than after the mechanical load-on. The data obtained up to now seems insufficient to explain the reason of this disparity.

It should be understood that the kinetic approach described by the equations (10.4), (10.5), and (10.7) is probably not the only one possible. Real processes inside heterogeneous medium subject to external influences must include various nonlinear mechanisms. An adequate physical description must be based on additional experiments where the inner properties of media will be varied, as well as external influences.

The above experiments also provided the answer to the following question: does the shape of the seismograms and/or their spectra change after water infusion? To this end, several signals were selected which occurred practically at the same locations before and after water infusion. The search area was restricted by several centimeters around the bottom of the hole. Another requirement was approximate amplitudes of signals. With these quite rigid restrictions, several pairs of signals were selected.

Example of such signals can be seen in Fig. 10.16. The sources were located about 2 cm from the hole; the hypocenters were coincident within 1 cm. The lower oscillogram in Fig. 10.16 was recorded in the Initiation #1 before the water infusion; the upper one – 6 minutes after the water infusion; the amplitudes of the signals were practically identical. The structure of the oscillograms consists of 2 parts. In the first part, the high frequency oscillations can be seen during ~30

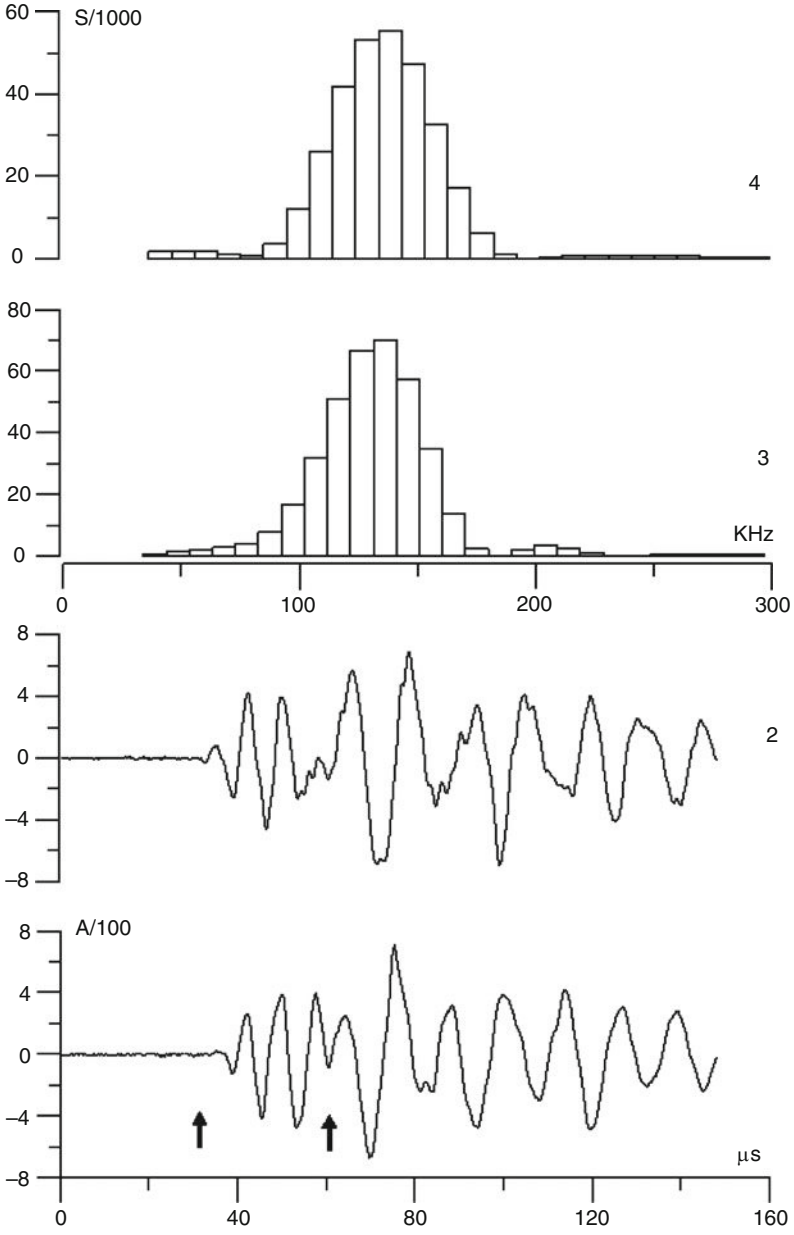

Fig. 10.16 Acoustic waveforms (1 and 2) and amplitude spectra for their initial parts (3 and 4) before water infusion (1 and 3) and after water infusion (2 and 4). Arrows show the time interval for spectra analysis

microseconds. Then these oscillations become lower-frequency ones. Having recorded and processed several hundreds of such signals, we came to the conclusion that the first part of the seismogram carries more information about the signal source and that information about the media is less pronounced in this part. The frequency composition is widely variable within 10^3–10^2 kHz, depending on the distance and azimuth between the source and the sensor. The second part basically reflects the oscillations of the sensor and adjacent parts of the model. The frequencies in this part of the signal were concentrated in the narrow 80–90 kHz range.

Two upper plots of Fig. 10.16 show the spectral densities calculated from the fist parts of the oscillograms; the intervals are indicated with arrows near plot 1; the spectral maxima are located near the ~130 kHz frequencies. The maxima for the second parts of oscillograms are equal to 86 kHz. Analysis of this pair and another pairs of signals did not yield any substantial differences in the waveforms or in the spectra of signals before and after the water infusion. This means that the influence of water did result in the decreased values of strength or in the increased values of local stresses, but dynamic "frictional sliding" occurred over the "dry" material, whose properties did not change significantly after the water infusion. It should be stressed that our experimental setup and conditions were substantially different from the majority of other experiments (laboratory as well as field ones) which are routinely conducted in the studies of hydrofractures. The effect of the pore pressure on the strength was insignificant, if present at all. The AE initiation in our case was due to the physical-chemical interaction of the solid and liquid interval for which the spectra were calculated. In the experiments described here AE signals with high energy always occurred after smaller events, aftershock activity was almost nonexistent, and the activity itself had a clustered dynamics. The latter feature is probably caused by the penetration of water into the areas of metastable cracks. The sizes of the AE emitting cracks can be indirectly estimated as follows. In the paper [Kuksenko, 1983] it was discovered that the length L of a crack developing with a constant velocity V is directly proportional to the pulse build-up τ of the AE signal thus emitted

$$\mathrm{L(mm)} = \mathrm{a}\cdot\mathrm{C(mm/\mu s)}\cdot\tau(\mu\mathrm{s}) \tag{10.9}$$

where a is some dimensionless factor close to 1. The pulse build-up of the majority of AE signals in Fig. 10.16, depending on the amplitude of the signal, was in the range 1-3 microseconds. Assuming the average velocity of crack development in the weakened area of the model C ~= 1 mm/microsecond, the crack sizes can be estimated at 1-3 mm.

10.5 Conclusions

The series of long-term experiments show that at a constant stress level the infusion of a relatively small volume of water (0.1% of the model) results in the activation of AE emission, which does not contradict the theory of the triggered mechanism of AE activation.

AE emissions of greater energy emerge after the initial smaller events; the sequence of different-energy events resembles the swarm which is observed in seismically active areas.

The AE activity emerges at different moments in different areas of the deformed model; this is caused by the different times of fluid inflow to the active cracks and by differences in local stresses.

There are no significant differences in the waveforms and in the spectral composition of AE signals recorded before and after the water infusion; this fact suggests the local decrease of material strength and/or the local increase of stresses near the metastable cracks.

The relaxation dynamics of AE processes after the load-ons and after initiation by water infusion is substantially different. In the first case it corresponds to the Omori law, whereas in the second case the AE activity has a clearly defined maximum.

Applying the kinetic approach to a medium with the finite number of metastable cracks allows to describe the AE dynamics caused by water infusion.

References

Brace WF., Martin RJ. A test of the law of effective stress for crystalline rocks of low porosity // Intern. J. Rock Mech. Mining. Sci. 1968, Vol. 5, p. 415–426.

Djadkov P.G. Induced Seismicity at the Lake Baikal: Principal Role of Load Rate. The 29-th General Assembly of the International Association of Seismology and Physics of the Earth's Interior, August 18-28, 1997, Thessaloniki, Greece, Abstracts, p. 359.

G.A. Sobolev, A.V. Ponomarev, A.V. Kol'tsov, A.A. Kruglov, V.A. Lutsky, and Yu.V. Tsyvinskaya. The effect of water injection on acoustic emission in a long-term experiment. Geology and Geophysics. 2006, Vol. 47, No. 5, pp. 608–621.

Gupta H.K., Reservoir-Induced Earthquakes, Elsevier, Amsterdam, 1992, p. 364).

Kornev V.M. The quantitative description of Rebinder effect (fragile and quasifragile materials) from retarding destruction to spontaneous dispersion. The physical mesomechanics, 2003, Vol. 6, No 3, p. 9–18, (in Russian).

Kuksenko V.S. et al. The estimation of dimensions of growing cracks and zones of unloading with parameters of acoustic signals. The mechanic of composite materials. 1983, No. 3, p. 536–543, (in Russian).

Miller S.A., Y. Ben-Zion, J. Burg. A three-dimensional fluid-controlled earthquake model: Behavior and implications. J.Geoph.Res., 1999, Vol. 104, No. B5, p. 10621–10638.

Mirzoev K.N., Negmatulaev SKh., D. Simpson &others. The induced seismicity in the region of the Nurek GES reservoir. Dushanbe, M. Donish, 1988, p. 402, (in Russian).

Peinke J., Matcharashvili T., Chelidze T., Gogiashvili J., Nawroth A., Lursmanashvili O., and Javakhishvili Z., "Influence of Periodic Variations in Water Level on Regional Seismic Activity Around a Large Reservoir:Field and Laboratory Model," Phys. Earth Planet. Inter., **156** (1–2), 130–142 (2006).

Rehbinder P.A., Shchukin E.D. The surface effects in solid materials during processes their deformation and failure. The successes of physical sciences. 1972, T. 108, p. 3–42, (in Russian).

Scholz C.H., Sykes L.R., Aggarwall Y.P. Earthquake prediction: A physical basis. Science. 1973. Vol. 181, p. 803–810.

Simpson, D., Leith, W., Scholz, C.: Two types of reservoir- induced seismicity. Bull. Seismol. Soc. Am. 78, 2025–2040, 1988.

Smirnov V.B., A.S. Cherepantsev, V.K.Mirzoev. The fractal properties of induced seismicity in the region of Nurek reservoir. The induced seismicity. M. Nauka, 1994, (in Russian).

Sobolev G.A., Ponomarev A.V. The method of detection of instability of the geological medium model. DAN, 1997, Vol. 356, No 4, p. 541–544, (in Russian).

Sobolev G.A., Ponomarev A.V. The physic of earthquakes and forerunners. M., Nauka, 2003, p. 270, (in Russian).

Sobolev G.A. Fundamental of Earthquake Prediction. Moscow. 1993, 313 p, (in Russian).

Stavrogin A. N. and Protosenya A. G. The Strength of Rocks and the Competence of Workings at Large Depths. Nedra, Moscow, 1985, pp. 1–272. (in Russian).

Tamuzh V. P. and Kuksenko V. S. Micromechanics of the Polymer Materials' Destruction. Zinatne, Riga, 1978, pp. 1–295. (in Russian).

Traskin V.U., Pertsev N.V., Kogan I.S. The influence of water on mechanic properties and disperse structure of rocks., In book The water in disperse systems. M. Khimia, 1989, p. 83–100, (in Russian).

Trifu, C.I. (ed.): The mechanism of induced seismicity, special volume. Pure Appl. Geophys. 159 (2002).

Zhurkov S.N. Kinetic concept of the strength of solids. Int. J. Fracture 1984, Vol. 26, No 4, p. 295–307.